Morphology-independent stable white-light emission from self-assembled two-dimensional perovskites driven by strong exciton–phonon coupling to the organic framework

Thirumal, Krishnamoorthy; Chong, Wee Kiang; Xie, Wei; Ganguly, Rakesh; Muduli, Subas Kumar; Sherburne, Matthew; Asta, Mark; Mhaisalkar, Subodh Gautam; Sum, Tze Chien; Soo, Han Sen; Mathews, Nripan

2017

Thirumal, K., Chong, W. K., Xie, W., Ganguly, R., Muduli, S. K., Sherburne, M., . . . Mathews, N. (2017). Morphology-independent stable white-light emission from self-assembled two-dimensional perovskites driven by strong exciton–phonon coupling to the organic framework. Chemistry of Materials, 29(9), 3947-3953. doi:10.1021/acs.chemmater.7b00073

https://hdl.handle.net/10356/142521

https://doi.org/10.1021/acs.chemmater.7b00073

Morphology Independent Stable White-Light Emission from Self-Assembled 2D Perovskites Driven by Strong Exciton-Phonon Coupling to the Organic Framework

Krishnamoorthy Thirumal,[†,#,‡] Wee Kiang Chong,[€,¥,‡] Wei Xie,[§] Rakesh Ganguly,[#] Subas Kumar Muduli,[†] Matthew Sherburne,[§] Mark Asta,[§] Subodh Mhaisalkar,[†,∥] Tze Chien Sum,[,¥] Han Sen Soo,[#] Nripan Mathews[*,†,∥]*

[†]Energy Research Institute @NTU (ERI@N), Research Techno Plaza, X-Frontier Block, Level 5, 50 Nanyang Drive, Singapore 637553

[#]Division of Chemistry and Biological Chemistry, School of Physical and Mathematical Sciences, Nanyang Technological University, 21 Nanyang Link, Singapore 637371

[€]Energy Research Institute @ NTU, ERI@N, Interdisciplinary Graduate School, Nanyang Technological University, Singapore

[¥]Division of Physics and Applied Physics, School of Physical and Mathematical Sciences, Nanyang Technological University, 21 Nanyang Link, Singapore 637371

[‖]School of Materials Science and Engineering, Nanyang Technological University, Nanyang Avenue, Singapore 639798

[§]Department of Materials Science and Engineering, University of California, Berkeley, CA 94720.

Abstract

Hybrid two-dimensional (2D) lead halide perovskites have been employed in optoelectronic applications, including white light emission for light emitting diodes (LEDs). However, until now, there have been limited reports on white light emitting lead halide perovskites with experimental insights into the mechanism of the broad band emission. Here, we present white light emission from a 2D hybrid lead chloride perovskite, using the widely known phenethylammonium cation. The single crystal X-ray structural data, time-resolved photophysical measurements, and DFT calculations are consistent with broad band emission arising from strong exciton-phonon coupling with the organic lattice, which is independent of surface defects. The phenethylammonium lead chloride material exhibits a remarkably high color rendering index of 84, CIE coordinate of (0.37,0.42), CCT of 4426, and photostability, making it ideal for natural white LEDs applications.

Artificial white-light has been traditionally used and produced by incandescent light bulbs and fluorescent lamps.[1] Light emitting diodes (LEDs) have become more widespread due to their higher electrical to luminance efficiencies, which are crucial to achieve energy sustainability. However, broadband white LEDs typically comprise of UV or blue LEDs coated with a single yellow or multiple phosphors.[2] This conventional approach is undesirable since the spectral overlap of different phosphors can result in self-absorption and hence losses in emission efficiencies. Moreover, progressive color changes may occur due to disparate aging rates of the phosphors. Consequently, the development of a single, broadband emitting, highly luminescent, and photostable material is an attractive objective for practical implementation.

Over the past decade, hybrid organic-inorganic halide perovskites have been rediscovered and applied in burgeoning optoelectronic fields including, but not limited to, solar cells, non-linear optics, and lasers.[3-9] In particular, lead (and tin) halide perovskites have shown remarkable color rendition tunability and good quantum efficiencies of photoluminescence emission, establishing them as suitable candidates for LEDs.[4, 10-12] Recently, Karunadasa and co-workers reported white-light emission from two instances of two-dimensional (2D) layered perovskites, (*N*-MEDA)PbX_4 (*N*-MEDA = N^1-methylethane-1,2-diammonium) and (EDBE)PbX_4 (EDBE = 2,2'-ethylenedioxy)bis(ethylammonium) with X = Cl or Br.[13-14] The origin of the white-light emission was attributed to electron-phonon coupling and self-trapped excitons.[13, 15] In addition, Yangui *et al.* conducted in-depth experimental investigations on the white-light emission behavior in thin films of cyclohexylammonium lead bromide $(C_6H_{11}NH_3)_2PbBr_4$.[15] The authors proposed that the luminescence arises from self-trapped states with energy barriers of approximately 10 meV. These self-trapped excitons were mostly attributed to excitons localized in the inorganic lattice. Herein, we report broad white light emission from the solution processed phenethylammonium

lead chloride $(C_6H_5C_2H_4NH_3)_2PbCl_4$ (hereafter as PEPC). This phenomenon is unexpected since only a narrow excitonic emission is observed for the bromide and iodide analogues of the phenylethylammonium systems.[16] We combine single crystal X-ray structural analyses, Raman spectroscopy, and steady-state, time-resolved, and temperature dependent photophysical studies to demonstrate that the broad emission is due to strong exciton-phonon coupling to the organic framework. These suggest that the organic framework is not acting merely as an inert spacer, and choosing the right combination of both the inorganic and organic components is important for white emission.

Results and Discussion

Four different forms (single crystal, powder, thin film and nanoparticles) of PEPC were prepared for evaluating their white light emission property and to trace the origin of white-light emission. Single crystals of the compound were prepared by using anti-solvent vapor assisted crystallization, in which PEPC was dissolved in DMF and nitromethane was used as an anti-solvent. In this growth process, the vapor of nitromethane was allowed to slowly diffuse into the perovskite solution which resulted in the formation of good quality single crystals of PEPC within a week. **Figure 1** shows the unit cell of PEPC and Tables S1 – S6 summarize the crystallographic and refinement data. PEPC crystallizes in the triclinic space group P-1, consistent with a previous report.[17] Interestingly, the unit cell for PEPC is isomorphic with the triclinic $(C_6H_5C_2H_4NH_3)_2PbBr_4$ (PEPB), but not with the monoclinic $(C_6H_5C_2H_4NH_3)_2PbI_4$. The 2D nature of PEPC in the ab plane is illustrated in **Figure 1**. Ordered layers of corner sharing $PbCl_6^{4-}$ octahedra are sandwiched between the phenethylammonium cation layers, which are stacked contiguously without interleaving. Each layer contains two different type of Pb atoms

with different environments (**Figure S1a & b**). Thin films of PEPC were prepared by spin coating 0.20 M perovskite solution prepared in DMSO followed by annealing at 100 ℃, while powder samples were prepared by dropcasting and grinding under same conditions. X-ray diffraction (XRD) data confirmed the phase purity and crystallinity (**Figure S4, Figure S6**) of both the samples. Thermogravimetric (TGA) and differential scanning calorimetry (DSC) (**Figure S5**) analysis on this material shows that PEPC is stable beyond 100 ºC. XRD measurements of the thin films (**Figure S6a**) display only the (00*l*) diffraction peaks, which indicate the formation of highly oriented perovskite planes parallel to the substrate surface. **Figure 2a** shows that the film forms a micro-disk like morphology with an average lateral size of 3 μm. Atomic force microscopy (AFM) (**Figure S7**) confirms the thicknesses of the disks to be around 60 nm. Addition of ligands is expected to reduce the ripening of the nuclei and result in more nucleation sites. Overall, this will result in the formation of smaller nanostructured materials. Octylamine was utilized as a capping ligand, however non-optimal concentrations of the ligand resulted in the formation of the octylammonium lead chloride (C8LC) perovskite along with formation of PEPC nanoparticles. The XRD pattern in **Figure S6b** shows the peaks at 2θ values of 8.37° and 12.56°, which account for the formation of C8LC. Hence, the ligand concentration was systematically reduced to 0.060 mmol, which allowed the formation of PEPC nanoparticles alone. Poor solubility of PEPC in DMF could induce more nucleation sites, which reduces the amount of perovskite in the mother liquid available for the further growth of the nuclei hence small amount of ligand is enough to stop the growth of nanoparticles and ultimately produce nanoparticles with average sizes of 10 nm. The XRD data of the nanoparticles concurs with that of the thin film. The interplanar spacing of PEPC was calculated as 1.67 nm based on the high intensity peak at the low 2θ value of 5.27° indicating that these nanoparticles contain six

layers of lead(II) chloride. **Figure 2b** shows the transmission electron microscope (TEM), image of the PEPC nanoparticles that are clearly different from the micro-platelets obtained for PEPB. Almost spherical nanoparticles with sizes ranging from 2 to 20 nm can be observed, although most of the particles average between 5 and 8 nm. The high resolution transmission electron microscopy (HRTEM) image as shown in **Figure S8a** displayed lattice fringes of 0.282 nm, which can be indexed to the (006) plane of the triclinic PEPC. The d-spacing in the PEPC nanoparticles was calculated using the reciprocal lattice of the selected area electron diffraction (SAED) pattern in **Figure S8b**, and agreed with the value calculated from the powder XRD data. The photoluminescence quantum efficiency PLQE of PEPC in various forms was measured and found to be less than 1 %.

Figure 2c shows the absorption spectra of a PEPC thin film and a nanoparticle solution in toluene. The strong excitonic nature of the samples, as a result of dielectric confinement, give rises to a sharp absorption peak at ~ 340 nm which is characteristic of 2D lead halide perovskites.[18] Upon resonantly irradiating the excitonic state with 340 nm UV femtosecond pulses, a broad photoluminescence (PL) peak spanning ~ 400 nm to ~ 900 nm can be observed for each of the PEPC nanoparticles solution, powder, thin film, and single crystal samples **(Figure 2d)**. A photograph of the emission from a thin film is shown in the **Figure 2d** inset. The PL spectra for these samples are nearly invariant and these data suggest an intrinsic origin to the broad emission. The PL spectrum excited using a 340 nm continuous wave excitation (generated using a xenon arc lamp) shows a peak blue-shifted with CIE 1931 coordinates in the white region **(Figure S10a, b and c)**. On the contrary, the CIE 1931 coordinates for the emission excited with femtosecond pulses was found to be in the yellow to orange region on the CIE 1931 color space

instead **(Figure S10b)**. CW excitation causes significant lattice heating, which introduces higher degrees of interband phonon absorption that blue-shifts the peak (**Figure S11**). The PL lifetimes measured at the peak position (~545 nm) for the thin film, powders, and nanoparticle solution samples were found to be similar with an average lifetime (amongst these samples) to be 4.2 ± 0.9 ns **(Figure 3e)** and also suggest that the surface-to-bulk ratio has little influence to the decay kinetics. The time-resolved PL (TRPL) spectra for a PEPC single crystal measured at three different wavelengths (480, 545, and 610 nm) were also found to be similar with an average lifetime of 3.0 ± 0.4 ns, which suggest emission from the same origin **(Figure 3f)**. These results confirm the intrinsic nature of the broad emission.

Previously, Ueda *et al.* has reported the disorder in the orientation of phenethylammonium cations in PEPC using ^{1}H and ^{13}C NMR studies.[19-20] Different orientations of PEA cations could possibly affect the band structure of PEPC dramatically and could be a source of the white light emission. We have thus conducted density functional theory (DFT) calculations to examine the effects of the orientation on the band structure. DFT calculations based on the generalized gradient approximation (GGA) predict that PEPC should have a direct band gap at the origin of the Brillouin zone, Γ **(Figure S3)**. Our calculations based on DFT-GGA underestimate the band gap by about 1.4 eV when spin orbit coupling (SOC) and van der Waals (vdW) corrections are included, compared to the experimental optical band gap value of 3.56 eV **(Table S7)**. However, the relative predicted band characters should be realistic. Although most frontier electronic bands disperse significantly, some up to about 1 eV along directions in or close to the inorganic layer, those along the stacking direction (Γ-M in **Figure S3**) are much flatter, and in some cases approximately constant throughout the Brillouin zone**.** This feature of nearly dispersionless bands in the direction perpendicular to the layers has been observed and suggested to correspond

to poor inter-layer charge transport in many previous studies of related 2D hybrid perovskites.[21-25] Near the valence band maximum (VBM), the bands are predominantly of Pb 6s character with some hybridization with Cl 3p states, while those near the conduction band minimum (CBM) have predominantly Pb 6p character, again with some hybridization with Cl 3p states. As in other Pb containing hybrid perovskites, SOC has a large effect on the electronic structure of PEPC, leading primarily to a lowering of the energies of Pb 6p states and their hybridized Cl 3p states with respect to VBM, hence reducing the band gap by 0.7-0.9 eV for PEPC.

The vdW interactions also affect the electronic structure, presumably due to their substantial effect on the inter-layer spacing. Without vdW corrections, DFT-GGA significantly overestimates the atomic volume and interlayer lattice constant *c* relative to experimental measurements, as shown in Table S7, which indicates that vdW interactions play a large role in maintaining the structure of such 2-D layered materials.[26] As a result of the significant change in lattice constant, the band gap is also reduced by about 0.1 eV when vdW corrections are included in the calculations. The bands near the VBM and CBM show negligible contributions from the organic PEA cations **(Figure S3)**. However, the different orientations of the PEA cations are found to affect mainly the energy of Pb 6s valence bands, leading to changes of the band gap and also the total energy of PEPC. More specifically, Pb 6s bands are more energetically dispersive when they are in orientation 2 compared to orientation 1 (see panels (c) and (d) of **Figure S3**), while the conduction bands on the other hand are observed to be less affected. The net effect is that the band gap is decreased by merely 2.27 - 2.11 = 0.16 eV, and the total energy is increased by 0.638 eV/cell in orientation 2, as calculated with DFT-GGA including SOC and vdW corrections. Thus, the band gap fluctuation (587 nm - 546 nm = 40 nm) induced by disordered orientation of organic cation is unlikely to be the main cause of the broadband white-light

emission, which extends from 400 nm to 900 nm. However, this band gap fluctuation could play a role in broadening the photoluminescence spectrum.

The decay profiles of PEPC single crystals for the respective laser fluences are shown in **Figure 3a**, with little variation in the kinetics with increasing laser fluence (**Figure S12**). The nature of the species contributing to the broad emission can be investigated by monitoring the change of peak TRPL intensity with laser fluence. A linear dependence between the initial time PL intensity and the laser fluence measured at 480, 545 and 610 nm (**Figure 3b**) can be observed, which suggests unimolecular excitonic recombination taking place. The similar linear trends observed for these three wavelengths also support the assignment of broad emission from identical species. The lack of steady-state PL saturation from the PEPC single crystals also suggests that the emission is not likely to be solely trap-related[27] **(Figure S13)**.

Figure 4a shows the temperature dependent PL spectrum of PEPC single crystals. As the temperature is lowered, the emission intensity increases with a slight narrowing of the full-width at half maximum wavelength (FWHM) **(Figure 4a inset)**. However, such changes do not introduce significant change in the CIE 1931 chromaticity coordinates when the temperature is lowered **(Figure S14)**. Two main processes (with two activation energies) were found to be responsible for the increase in integrated PL intensity with decreasing temperatures **(Figure 4b)**. The activation energies were obtained using Arrhenius fitting (with a minimum of two exponentials – See **Figure S15** for fitting details) with the form:

$$I(\mathrm{T}) = \frac{I_0}{1 + Ae^{-\frac{E_A}{k_B T}} + Be^{-\frac{E_B}{k_B T}}} \quad (1)$$

where I_0 is the integrated PL intensity at $T = 0$ K, A and B are the pre-exponential amplitudes, k_B is the Boltzmann constant, and E_A and E_B are the average activation energies responsible for the

broad emission. The fitting yields an adjusted R-squared value of 0.997. The first process, having a small activation (E_A) of 12 ± 1 meV, is likely to be a bound exciton de-trapping process. Below 140 K (or equivalently 12 meV), these bound excitons do not have sufficient energy to be converted back to free excitons, giving rise to a higher bound exciton PL intensity. This small activation energy is also comparable to previously reported value in broad emitting 2D perovskite[15]. On the contrary, the second process possesses a much larger activation energy (E_B) of 120 ± 10 meV. This large energy can be interpreted to be: (a) the energy difference between a free exciton and a bound excitonic state or (b) the energy difference between a bound excitonic state and the conduction band minimum or (c) the energy of phonons responsible for non-radiative recombination. Both hypotheses (a) and (b) can be eliminated since the binding energy in PEPC systems is at least ~ 400meV[28]. We propose that (c) is likely to be responsible for the large activation energy of 120 ± 10 meV (or 968 ± 80 cm^{-1}) as this energy corresponds well to an organic phonon mode[29] measured using Raman spectroscopy **(Figure S16)**. Therefore the decrease in PL intensity at higher temperatures is likely due to increased non-radiative recombination (indirect recombination) caused by phonon absorption **(Figure S11 – green arrows)**. The increased non-radiative recombination is also reflected in the temperature dependent PL spectrum where significant lifetime shortening is observed at higher temperatures **(Figure S17)** and could also possibly account for the low PLQE of PEPC at room temperature. In addition, the increased non-radiative recombination at higher temperatures could also be due to effects from thermal energy (25 meV) and/or tunneling processes (probabilistic process with little activation energy required), even though they are not reflected strongly in our experimental findings. The broadening in FWHM with increasing temperature can be attributed to carrier scattering process and can be described using the equation[14]:

$$\Gamma(T) = \Gamma_0 + \Gamma_{LO}(e^{E_{LO}/k_B T} - 1)^{-1} + \Gamma_{Inh} e^{-E_A/k_B T} \quad (2)$$

where Γ_0 is the FWHM at T= 0 K, Γ_{LO} is the exciton-LO phonon coupling constant, E_{LO} is the longitudinal-optical phonon energy and Γ_{Inh} is the inhomogeneous broadening coefficient. The second and third terms account for exciton-phonon coupling and inhomogenous broadening (due to the self-trapping) interaction terms respectively. Herein, we assume that the bound exciton trapping originates from defects responsible for FWHM inhomogeneous broadening. A good fit (with an adjusted R-squared value of 0.995) can be obtained using the parameters Γ_0 = 581 meV, Γ_{LO} = 265 ± 80 meV, E_{LO} = 54 ± 6 meV, Γ_{Inh} = 90 meV and E_A = 12meV **(Figure 4b)**. Three conclusions can be obtained from the fitting: (i) the value of Γ_{LO} is approximately twice as large compared to the value obtained from previous broad emitting 2D perovskite (130 ± 7 meV)[14] and comparable to ZnO quantum wells,[30] which suggests strong exciton-phonon coupling in PEPC, (ii) the LO phonon energy obtained from the fitting coincides well with the 60 meV Raman mode of the organic cation[29] **(Figure S16)**, which is a pre-requisite for exciton-phonon coupling to occur, and (iii) there exists a self-trapping potential barrier (~10 meV) for scattering. Since self-trapped excitons can be treated as bound excitons[27], the small activation obtained from Arrhenius equation fitting can therefore be assigned to self-trapping barrier energy. Unlike the conclusion by Hu *et al.*[13] where self-trapped excitons were attributed to solely the inorganic lattice, our findings indicate that there are major contributions from the organic framework. The PL spectrum in Figure 4a also undergoes less narrowing at lower temperature compared to Figure 4a of Reference 14. However, the spectral difference between this study and reference 14 cannot be used to determine to the self-trapping location. This is also the rationale of performing a fitting with equation (2) to extract both exciton-phonon coupling constant and phonon energy. It is the phonon energy that allows determination of the self-trapping location. As such, we

believe that both the organic and inorganic constituents are important for generating white emission. This is also supported by prior literature, where broad emission is observed by changing either the organic (e.g. (i) (*N*-MPDA)[$PbBr_4$] to (*N*-MEDA)[$PbBr_4$][24, 31] and (ii) PEPB to $(C_6H_{11}NH_3)_2PbBr_4$ [15]) or inorganic components (e.g. (i) PEPB[32-33] to PEPC (this work) and (ii) EDBE(PbI_4) to EDBE($PbCl_4$)[14]). Further evidence of self-trapped excitons can also be observed using transient absorption spectroscopy. **Figure 4c** shows the pseudocolor TA plot of PEPC single crystals as a function of probe wavelength and probe delay time. A broad featureless photo-induced absorption (PIA) plateau can be observed across the visible probe region **(Figure 4d inset)** and this is consistent with a previous report.[13] The kinetics probed at a few visible wavelengths (500, 600, and 700 nm) shows no significant changes in lifetimes **(Figure 4d)** and is consistent with the invariant PL lifetime measured at different wavelengths **(Figure 2f)**. The broad PIA plateau together with the invariant lifetimes suggest that the probed state cannot be directly excited and populated via transfer from intermediate states. This is also consistent with the self-trapped exciton assignment. In addition, the rise time of these PIA kinetics (limited by the laser pulse width) was fitted to be 100 fs. This value is in the same order of magnitude as the vibrational period of 69 fs (or 60 meV), which is the estimated formation time of the self-trapped excitons.

A broad emitting thin film that demonstrates good photostability and solution processability is ideal for white light emitting devices applications. PEPC, being a candidate that is solution processable, is attractive for this purpose. However, its photostability has not been reported. Therefore, the photostability of a PEPC thin film was assessed by monitoring the emission peak intensity as a function of time under UV fs laser irradiation in N_2 environment with fluence 2.1

$\mu J/cm^2$ at a 1 KHz repetition rate. After ~14 hours of continuous excitation (or 10^5 laser shots), the thin film showed no significant reduction of peak intensity **(Figure 5)** with a mean and standard deviation value of 0.98 and 0.05 respectively. This measurement demonstrates the photostability of PEPC thin films under UV excitation. This is in contrast to its bromide variant (PEPB) where poor photostabillity (a reduction in ~80% of PL peak intensity after ~6 hours) is observed with UV excitation **(Figure 4)**. The observation of poor photostability in PEPB under UV excitation has also been reported previously by Wei *et al*[34].

Conclusion

Our findings establish the ease of achieving room temperature white emission from various forms of PEPC. Notably, we report the first observation of white emission from 2D perovskite nanoparticles in this study. These solution-processed materials also possess high color rendering indices, good CIE coordinates, and excellent photo-stability, which are desirable for natural, white light LED applications. The broad-band emission was found to originate from self-trapped excitons predominantly in the organic lattice. This is in contrast to the commonly attributed origins of self-trapped excitons only in the inorganic metal halide lattice. Our findings highlight the importance of judiciously selecting both the organic and inorganic components in 2D perovskites for white light emission.

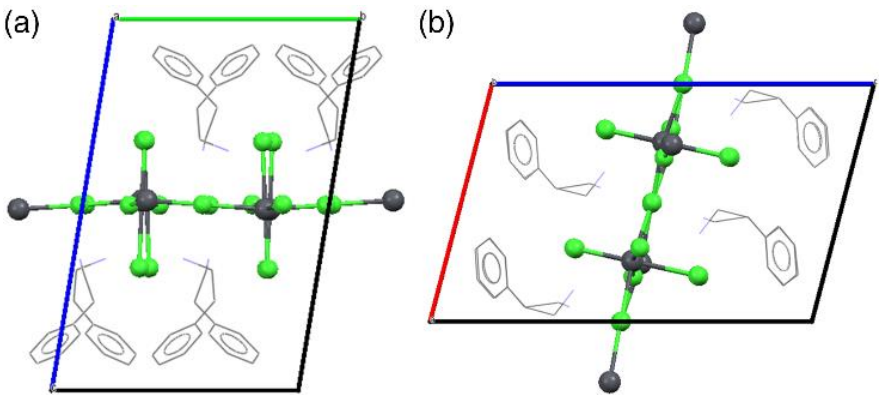

Figure 1. Structure of PEPC. Projection of PEPC viewed along the (a) a- and (b) b-axis, showing the organic ammonium cations intercalating between the 2D lead chloride layers. The Pb atoms are represented in grey, while the iodide atoms are in green.

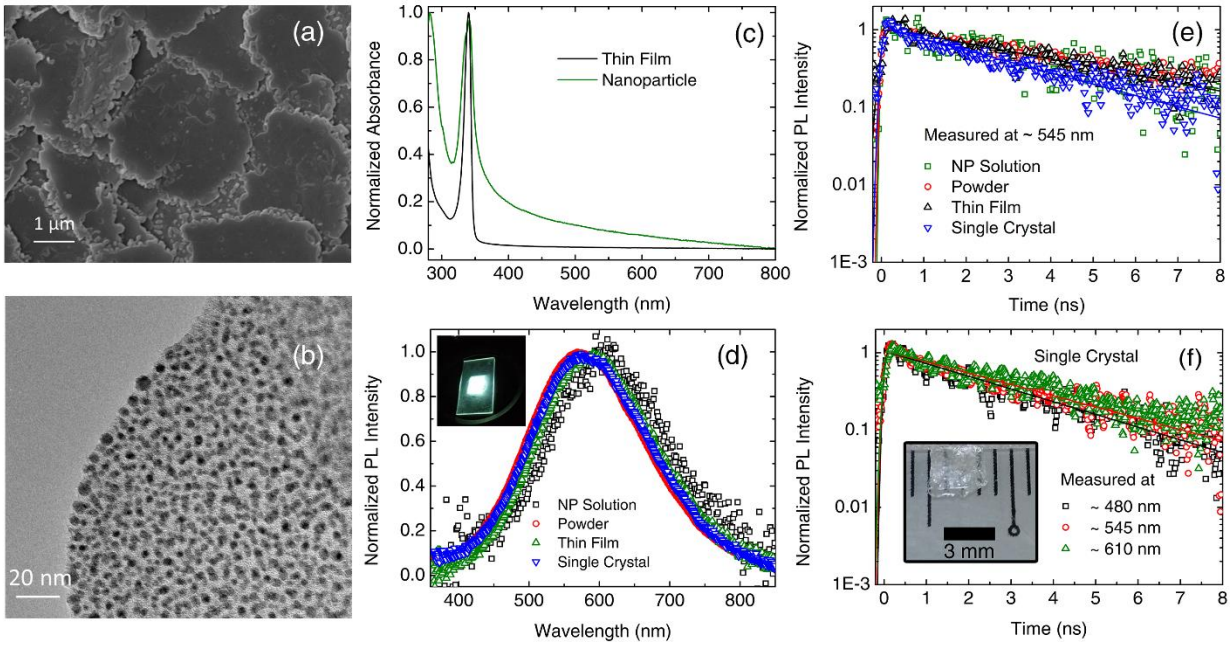

Figure 2. Strong excitonic absorption and intrinsic broad emission from PEPC. (a) FESEM of thin film produced using a 0.20 M solution of PEPC. (b) TEM image of PEPC nanoparticles. (c) Steady-State absorption spectra of PEPC samples, each showing a strong narrow absorption peak that is characteristic of a strongly confined excitonic system. (d) Steady-state PL spectra of

PEPC nanoparticles (NP) solution, powder, thin film, and single crystal samples, each showing a broad emission that spans ~400 nm to ~900 nm. The inset shows the photograph of the emission excited using 340 nm. (e) TRPL spectrum of the different samples measured at ~545 nm showing similar decay behavior. The experiments are conducted using 340 nm laser excitation (50 fs, 1 KHz, 7 μJ/cm^2 (time-integrated PL) or 15 μJ/cm^2 (time-resolved PL)). (f) TRPL spectra measured at emission wavelengths of 480, 545, and 610 nm and excited using a 340 nm beam with a laser fluence of 15 μJ/cm^2 for sample containing single crystals. There is no observable change in the average lifetime (~3 ns) among the various samples for the measured wavelengths. Inset shows a photograph of the single crystal with a dimension of ~ 3 mm x 3 mm.

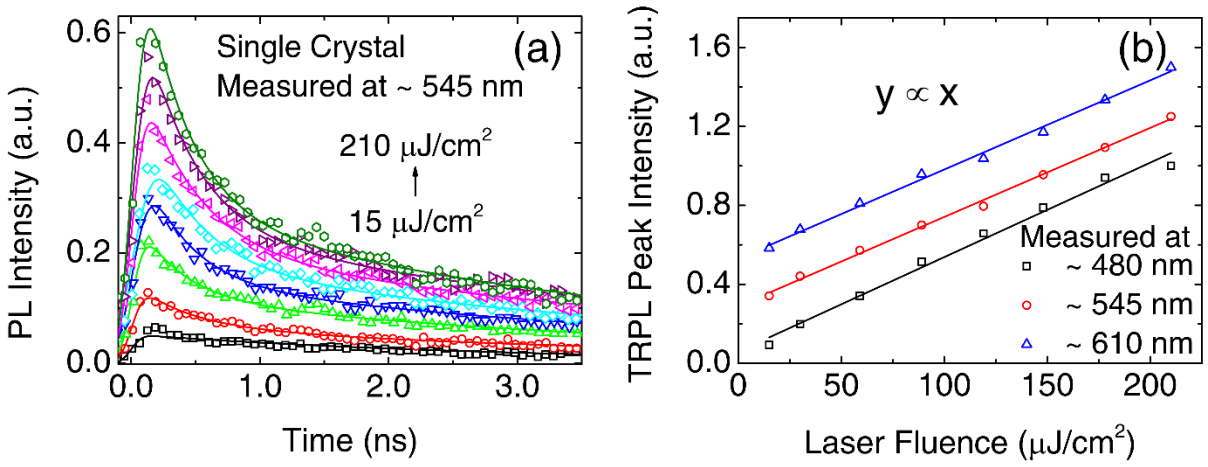

Figure 3. Monomolecular recombination (excitonic) in PEPC single crystals. (a) Laser fluence-dependent TRPL spectra of PEPC single crystals in the range of 15 to 210 μJ/cm^2 measured at 545 emission wavelength. (b) TRPL peak intensities as functions of laser fluences measured at 480, 545, and 610 emission wavelengths showing linear behavior. Each experiment is conducted using 340 nm laser excitation (50 fs, 1 KHz).

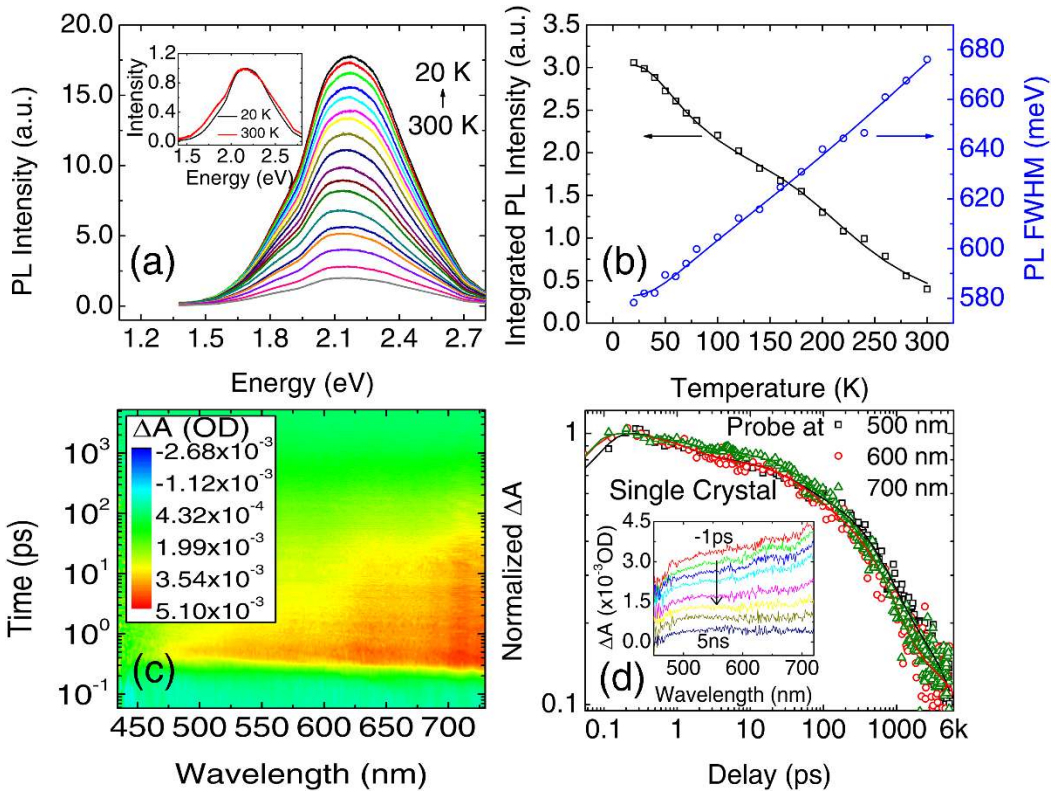

Figure 4. Self-trapped excitons in PEPC. (a) Temperature-dependent PL spectra of PEPC single crystals. Inset shows the overlaid normalized PL spectrum of PEPC at 20 K and 300 K. (b) Integrated PL intensity (black) and FWHM (black) as a function of temperature. The black and blue points are fitted with equation (1) and (2) respectively. The PL and TRPL measurements were conducted using 340 nm excitation and 3.5 μJ/cm^2 laser fluence (50 fs, 1 KHz). (c) Pseudocolor TA plot of PEPC Single crystal showing the change in absorption (ΔA) as a function of probe wavelength and probe delay time. (d) TA kinetics of PEPC single crystal probed at 500, 600, and 700 nm. Inset shows ΔA as a function of probe wavelength at selected delay time. The TA measurements were conducted using 340nm excitation and ~ 25 μJ /cm^2 laser fluence (150 fs, 1 KHz).

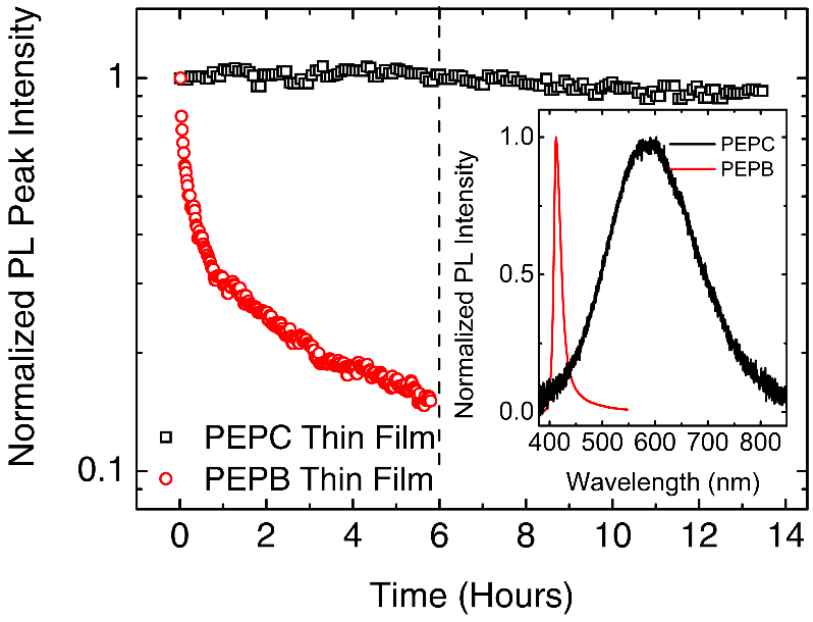

Figure 5. Photostability of PEPC and generation of near pure white emission. Room temperature PL peak intensity variation of with continuous 340 nm excitation for ~14 hours for PEPC and ~6 hours for PEPB in N_2 environment using a laser fluence of 2.1 μJ/cm^2. Inset shows the normalized PL spectrum of PEPC and PEPB at the time = 0 h.

Supporting Information. Experimental sections, single crystal structure and data, XRD, TGA, DSC, FESEM, PESA, TRPL, SSPL, CIE coordinate with variable temperature, Raman spectrum, and Temperature dependent PL. CIF for PEPC has been deposited in the Cambridge Crystallographic Data Centre under deposition number CCDC 1498513. This material is available free of charge via the Internet at http://pubs.acs.org.

AUTHOR INFORMATION

Corresponding Author

* Nripan@ntu.edu.sg; Tzechien@ntu.edu.sg

Author Contributions

‡These authors contributed equally.

ACKNOWLEDGMENT

Funding from the Singapore National Research Foundation through the Competitive Research Program NRF-CRP14-2014-03 and the Singapore–Berkeley Research Initiative for Sustainable Energy (SinBeRISE) CREATE Program is gratefully acknowledged. Financial support from Nanyang Technological University start-up grants M4080514, M4081293, and M4081012; the Ministry of Education AcRF Tier 1 grants RG184/14, RG101/15, and RG1/13; and Tier 2 grants MOE2014-T2-1-044 and MOE2015-T2-2-015; the NTU-A*STAR Silicon Technologies Center of Excellence Program Grant 11235100003. Extreme Science and Engineering Discovery Environment (XSEDE), which is supported by U.S. National Science Foundation grant number ACI-1053575 is also acknowledged. We thank Nguyen Huy Tiep for atomic-force microscopic (AFM) characterization and Dr. Saikat Bhaumik for inputs into nanoparticle synthesis.

REFERENCES

1. Kamtekar, K. T.; Monkman, A. P.; Bryce, M. R., Recent Advances in White Organic Light-Emitting Materials and Devices (WOLEDs). *Adv. Mater.* **2010**, *22*, 572-582.

2. Ye, S.; Xiao, F.; Pan, Y. X.; Ma, Y. Y.; Zhang, Q. Y., Phosphors in Phosphor-Converted White Light-Emitting Diodes: Recent Advances in Materials, Techniques and Properties. *Mater. Sci. Eng., R* **2010**, *71*, 1-34.

3. Krishnamoorthy, T., et al., Lead-Free Germanium Iodide Perovskite Materials for Photovoltaic Applications. *J. Mater. Chem. A* **2015**, *3*, 23829-23832.

4. Xing, G.; Mathews, N.; Lim, S. S.; Yantara, N.; Liu, X.; Sabba, D.; Grätzel, M.; Mhaisalkar, S.; Sum, T. C., Low-Temperature Solution-Processed Wavelength-Tunable Perovskites for Lasing. *Nat Mater* **2014**, *13*, 476-480.

5. Xing, G.; Mathews, N.; Sun, S.; Lim, S. S.; Lam, Y. M.; Grätzel, M.; Mhaisalkar, S.; Sum, T. C., Long-Range Balanced Electron- and Hole-Transport Lengths in Organic-Inorganic Ch3nh3pbi3. *Science* **2013**, *342*, 344-347.

6. Yuan, M., et al., Perovskite Energy Funnels for Efficient Light-Emitting Diodes. *Nat Nano* **2016**, 11, 872-877.

7. Klein-Kedem, N.; Cahen, D.; Hodes, G., Effects of Light and Electron Beam Irradiation on Halide Perovskites and Their Solar Cells. *Acc. Chem. Res.* **2016**, *49*, 347-354.

8. Lee, J.-W.; Kim, H.-S.; Park, N.-G., Lewis Acid–Base Adduct Approach for High Efficiency Perovskite Solar Cells. *Acc. Chem. Res.* **2016**, *49*, 311-319.

9. Manser, J. S.; Christians, J. A.; Kamat, P. V., Intriguing Optoelectronic Properties of Metal Halide Perovskites. *Chem. Rev.* **2016,** 116, 12956-13008.

10. Duan, H.-B.; Yu, S.-S.; Tong, Y.-B.; Zhou, H.; Ren, X.-M., Two in One: Switchable Ion Conductivity and White Light Emission Integrated in an Iodoplumbate-Based Twin Chain Hybrid Crystal. *Dalton Trans.* **2016**, *45*, 4810-4818.

11. Dursun, I., et al., Perovskite Nanocrystals as a Color Converter for Visible Light Communication. *ACS Photonics* **2016**, 3, 1150-1156.

12. Pathak, S., et al., Perovskite Crystals for Tunable White Light Emission. *Chem. Mater.* **2015**, *27*, 8066-8075.

13. Hu, T., et al., Mechanism for Broadband White-Light Emission from Two-Dimensional (110) Hybrid Perovskites. *J. Phys. Chem. Lett.* **2016**, *7*, 2258-2263.

14. Dohner, E. R.; Jaffe, A.; Bradshaw, L. R.; Karunadasa, H. I., Intrinsic White-Light Emission from Layered Hybrid Perovskites. *J. Am. Chem. Soc.* **2014**, *136*, 13154-13157.

15. Yangui, A., et al., Optical Investigation of Broadband White-Light Emission in Self-Assembled Organic–Inorganic Perovskite (C6h11nh3)2pbbr4. *J. Phys. Chem. C* **2015**, *119*, 23638-23647.

16. Chong, W. K.; Thirumal, K.; Giovanni, D.; Goh, T. W.; Liu, X.; Mathews, N.; Mhaisalkar, S.; Sum, T. C., Dominant Factors Limiting the Optical Gain in Layered Two-Dimensional Halide Perovskite Thin Films. *Phys. Chem. Chem. Phys* **2016**, *18*, 14701-14708.

17. Mitzi, D. B., A Layered Solution Crystal Growth Technique and the Crystal Structure of (C6h5c2h4nh3)2pbcl4. *J. Solid State Chem* **1999**, *145*, 694-704.

18. Pradeesh, K.; Nageswara Rao, K.; Vijaya Prakash, G., Synthesis, Structural, Thermal and Optical Studies of Inorganic-Organic Hybrid Semiconductors, R-Pbi4. *J. Appl. Phys* **2013**, *113*, 083523.

19. Takahiro Ueda, M. O., Katsuyuki Shimizu, Hiroshi Ohki, and Tsutomu Okuda, Ionic Motion of Phenethylammonium Ion in $[C_6h_5ch_2ch_2nh_3]_2pbx_4$ (X = C1, Br, I) as Studied by ^{L}h Nmr. *Z. Naturforsch* **1997**, *52a*, 502-508.

20. Takahiro Ueda, K. S., Hiroshi Ohki, and Tsutomu Okuda, ^{13}c Cp/Mas Nmr Study of Motion and Local Structure of Phenethylammonium Ion in [C6h5ch2ch2nh3]2pbx4 (X = Cl, Br, I). *Z. Naturforsch* **1998**, *53a*, 983-988.

21. Mosconi, E.; Amat, A.; Nazeeruddin, M. K.; Grätzel, M.; De Angelis, F., First-Principles Modeling of Mixed Halide Organometal Perovskites for Photovoltaic Applications. *J. Phys. Chem. C* **2013**, *117*, 13902-13913.

22. Cao, D. H.; Stoumpos, C. C.; Farha, O. K.; Hupp, J. T.; Kanatzidis, M. G., 2d Homologous Perovskites as Light-Absorbing Materials for Solar Cell Applications. *J. Am. Chem. Soc.* **2015**, *137*, 7843-7850.

23. Fraccarollo, A.; Cantatore, V.; Boschetto, G., Ab Initio Modeling of 2d Layered Organohalide Lead Perovskites. *J. Chem. Phys.* **2016**, *144*, 164701.

24. Kamminga, M. E.; Fang, H.-H.; Filip, M. R.; Giustino, F.; Baas, J.; Blake, G. R.; Loi, M. A.; Palstra, T. T. M., Confinement Effects in Low-Dimensional Lead Iodide Perovskite Hybrids. *Chem. Mater.* **2016**, *28*, 4554-4562.

25. Tsai, H., et al., High-Efficiency Two-Dimensional Ruddlesden–Popper Perovskite Solar Cells. *Nature* **2016**, 536, 312-316.

26. Saparov, B.; Mitzi, D. B., Organic-Inorganic Perovskites: Structural Versatility for Functional Materials Design. *Chem. Rev.* **2016**, *116*, 4558-4596.

27. Pelant, I.; Valenta, J., *Luminescence Spectroscopy of Semiconductors. [Electronic Resource]*; Oxford : Oxford University Press, 2012., 2012.

28. Zhang, S.; Audebert, P.; Wei, Y.; Lauret, J.-S.; Galmiche, L.; Deleporte, E., Synthesis and Optical Properties of Novel Organic-Inorganic Hybrid Uv (R-Nh3)2pbcl4 Semiconductors. *J. Mater. Chem.***2011**, *21*, 466-474.

29. Xie, M.; Qi, Y.; Hu, Y., Conformational Equilibrium and Hydrogen Bonding in Liquid 2-Phenylethylamine Explored by Raman Spectroscopy and Theoretical Calculations. *J. Phys. Chem. A* **2011**, *115*, 3060-3067.

30. Makino, T.; Segawa, Y.; Kawasaki, M., Analytical Study on Exciton-Longitudinal-Optical-Phonon Coupling and Comparison with Experiment for Zno Quantum Wells. *J. Appl. Phys* **2005**, *97*, 106111.

31. Dohner, E. R.; Hoke, E. T.; Karunadasa, H. I., Self-Assembly of Broadband White-Light Emitters. *J. Am. Chem. Soc.* **2014**, *136*, 1718-1721.

32. Jemli, K.; Audebert, P.; Galmiche, L.; Trippé-Allard, G.; Garrot, D.; Lauret, J.-S.; Deleporte, E., Two-Dimensional Perovskite Activation with an Organic Luminophore. *ACS Appl. Mater. Interfaces* **2015**, *7*, 21763-21769.

33. Kitazawa, N.; Aono, M.; Watanabe, Y., Temperature-Dependent Time-Resolved Photoluminescence of (C6h5c2h4nh3)2pbx4 (X= Br and I). *Mater. Chem. Phys* **2012**, *134*, 875-880.

34. Wei, Y.; Audebert, P.; Galmiche, L.; Lauret, J.-S.; Deleporte, E., Photostability of 2d Organic-Inorganic Hybrid Perovskites. *Materials* **2014**, *7*, 4789-4802.

Table of Contents.